การวิเคราะห์อินพุตอิมพีแดนซ์ของสายอากาศไมโครสตริป โดยใช้วิธีไฟไนท์อิลิเมนต์

นิรันดร์ คำประเสริฐ*
ภาควิชาวิศวกรรมอิเล็กทรอนิกส์และโทรคมนาคม
คณะวิศวกรรมศาสตร์ สถาบันเทคโนโลยีพระจอมเกล้าธนบุรี

บทคัดย่อ

วิธีไฟไนท์อิลิเมนต์ที่ง่ายและมีประสิทธิภาพได้นำมาใช้สำหรับการวิเคราะห์อินพุตอิมพีแดนซ์ของสายอากาศไมโครสตริปหลายรูปแบบ ซึ่งป้อนสัญญาณให้สายอากาศด้วยสายโคแอกเชียลและสายส่งไมโครสตริป สมการอินทิกรัลเชิงไฟฟ้าได้กำหนดขึ้นจากสมการแม็กซ์เวลล์และปรากฏการณ์ทางแม่เหล็กไฟฟ้า และทำการแก้สมการอินทิกรัลเชิงไฟฟ้านี้โดยใช้อิลิเมนต์พื้นฐานรูปสามเหลี่ยม ร่วมกับฟังก์ชันของกรีน ผลของการคำนวณที่ได้แสดงให้เห็นว่ามีความถูกต้องและตรงกับผลการวัด

* ผู้ช่วยศาสตราจารย์

An Analysis of the Input Impedance of the Microstrip Antennas Using the Finite Element Method

Nirun Kumprasert*

Department of Electronics and Telecommunication Engineering,

Faculty of Engineering, King Mongkut's Institute of Technology Thonburi

Abstract

A simple and efficient finite element method is used for analysis of the input impedance of the complex planar microstrip antennas with various shapes, which include coaxial probe feed and microstrip line feed. For the electric integral equation, the formulation is based on the Maxwell's equations and the electromagnetic phenomena. The electric integral equation is solved by adopting the triangular shaped basis element and using the Galerkin procedure. In the integral equation, Green's functions are used. Illustrative numerical representations that demonstrate the validity, versatility, and efficiency of the method are presented.

*Assistant Professor

I. INTRODUCTION

The popularity of planar microstrip antennas has steadily increased in the past decade because they posses a number of advantages such as low cost, low profile, small size, light weight, easy to fabrication, and cornformability with existing structures fabrication. During this time, microstrip antennas have become an important area of communication and have led to a major development in antenna theory. Usually, a radiating element of microstrip antenna, consisting of a very thin metallic, is fabricated on a dielectric substrate, which is backed by a metallic ground plane. Practically, there are two simple structures that are used to feed microstrip antenna. These are coaxial probe feeds, and microstrip line feeds. The coaxial-fed structure is often used in a single element because of the ease of matching its characteristic impedance to that of the antennas, while microstrip line-fed structure is often used in a microstrip array antenna.

A number of recent methods have reported on the subject of matching impedance for microstrip antennas [1]-[6]. These methods are not accurate when the substrate is thicker than about 0.024, are not adequate for predicting impedance variation with feed location, and cannot be applied to any geometries besides rectangles. A number of numerical analysis of the input impedances of microstrip antennas have been proposed. However, most of the methods either have restricted application or require a large computer memory and long computing time, e.g., the mode-matching technique and the transverse resonance method can only study structures of rectangular cross sections, and a numerical technique, e.g., the finite element method (FEM) can handle many arbitrary cross-sectional geometrics and provides a technique for accurate modeling of planar microstrip antenna.

The FEM in this paper is based upon a boundary condition, or integral equation formulation, with the unknown being the current on microstrip patches and wire feed lines plus their images in the ground plane. A set of vector integral equation is derived which governs the current distribution on the patch. This set of equation is then

solved, in which the patch current is expanded in term of a complete set of basis function. This method can be applied to arbitrary shapes. The antenna is fed by a coaxial probe and microstrip line. Details of the theoretical background and formulation are presented in section II. The numerical results are shown in section III.

II. THEORETICAL BACKGROUND AND FORMULATION

In this section, an integral equation for the surface current induced on a conducting surface (microstrip patch) S is derived from boundary conditions on the electric field. To solve the integral equation, a set of basic function and testing procedure is developed and used to derive the elements of the matrix equation.

A. Electric Field Integral Equation

For a harmonically time varying fields dependence of $e^{-i\omega t}$ have been assumed, the fields in nonhomogenous isotropic media, Maxwell's equations can be adopted here as

$$\text{curl}\,\boldsymbol{E} = \nabla \times \boldsymbol{E} = -\frac{\partial \boldsymbol{B}}{\partial t} = -\mu\frac{\partial \boldsymbol{H}}{\partial t} = i\omega\mu\boldsymbol{H} \quad (1)$$

$$\text{div}\,\boldsymbol{D} = \nabla \cdot \boldsymbol{D} = \nabla \cdot \varepsilon\boldsymbol{E} = \rho \quad (2)$$

$$\text{curl}\,\boldsymbol{H} = \nabla \times \boldsymbol{H} = J + \frac{\partial \boldsymbol{D}}{\partial t} = J - i\omega\varepsilon\boldsymbol{E} \quad (3)$$

$$\text{div}\,\boldsymbol{B} = \text{V - B} = \nabla \cdot \mu\boldsymbol{H} = 0 \quad (4)$$

where E is the electric field intensity, D is the electric flux density, H is the magnetic field intensity, B is the magnetic flux density, J is the source charge current density, ρ is the charge density, μ is the complex magnetic permeability, ε is the complex electric permittivity, $i = \sqrt{-1}$, and ω is the angular frequency. For consideration the electric field intensity may be taken the divergence of both sides of (3) as

$$\nabla \cdot \nabla \times \boldsymbol{H} = \text{V} \cdot (\boldsymbol{J} - i\omega\varepsilon\boldsymbol{E}) \quad (5)$$

For a vector identity (V • V x H = **0**), *(5)* reduces to

$$0 = \text{V} \cdot J - i\omega\nabla \cdot \varepsilon\boldsymbol{E} \quad (6)$$

Substituting (2) into (6), this reduces to

$$\nabla \cdot J = i\omega\rho \tag{7}$$

Taking the curl of both sides of (1)

$$\nabla \times \frac{1}{\mu}\nabla \times \boldsymbol{E} = i\omega\nabla \times H \tag{8}$$

Substitution (3) into (8) yields

$$\nabla \times \frac{1}{\mu}\nabla \times \boldsymbol{E} - \omega^2\varepsilon\boldsymbol{E} = i\omega\boldsymbol{J} \tag{9}$$

For a boundary value problem (BVP), the field equivalence principle [7] is adopted here by considering an actual radiating source (antenna), which is electrically represented by electric current density $\boldsymbol{J}_1$ and magnetic current density $\boldsymbol{M}_1$ as shown in Figure 1 (a).

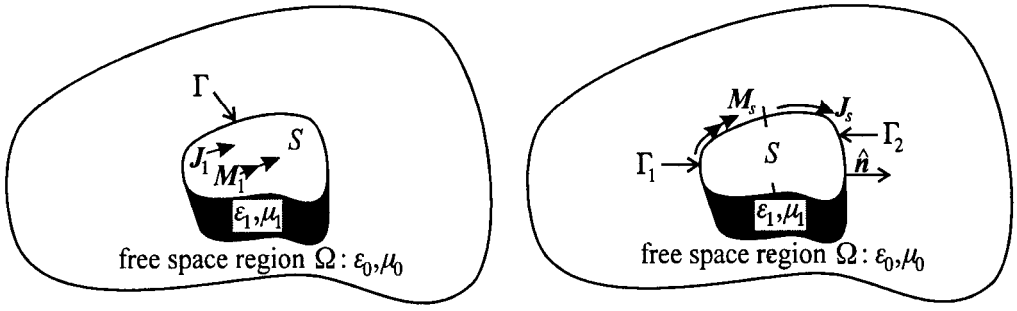

Γ : arbitrarily conducting boundary

Γ_1: electric conducting boundary

Γ_2: magnetic conducting boundary

(a) Actual problem (b) Equivalent problem

Figure 1. Arbitrarily shaped microstrip patch antenna.

In above case, the equivalent problem of Figure 1 (b), an actual radiating source radiate between the nonhomogenous isotropic media (ε_1, μ_1) and free space region Ω, the boundary value problem to be solved is to satisfy boundary conditions on the tangential electric and magnetic field components. The desired boundary value problem is to satisfy (2) and (9), in Ω, with the first boundary condition on *E* is

$$-\hat{n} \times \boldsymbol{E} = \boldsymbol{M}_s \text{ on } \Gamma_1 \tag{10}$$

and the secondary condition on $\boldsymbol{E}$ is

$$\frac{1}{i\omega\mu}\hat{\boldsymbol{n}} \times \nabla \times \boldsymbol{E} = \boldsymbol{J}_s \text{ on } \Gamma_2 \tag{11}$$

where $\boldsymbol{M}_s$ and $\boldsymbol{J}_s$ are equivalent current densities, and $\hat{\boldsymbol{n}}$ is an outward unit vector normal to the boundary of arbitrary surface S.

To formulate problem of Figure l(b), the arbitrary surface may be replaced by its equivalent, in which the electric conducting patch (surface) $\boldsymbol{S}$ has been removed, and magnetic vector potential $\boldsymbol{A}$ is useful in solving for the electric field generated by a given harmonic electric current density $\boldsymbol{J}_s$. ***The*** magnetic and electric field, $\boldsymbol{H}$ and $\boldsymbol{E}$, respectively, due to $\boldsymbol{J}_s$, in the above equations can be given as

$$\mu_o \boldsymbol{H}(\boldsymbol{r}) = \text{V x } \boldsymbol{A}(\boldsymbol{r}) \tag{12}$$

$$\boldsymbol{E}'' (\boldsymbol{r}) = i\omega \boldsymbol{A}(\boldsymbol{r}) - \nabla\Phi(\boldsymbol{r}) \tag{13}$$

where $\boldsymbol{E}^{in}(\boldsymbol{r})$ is the incident field on the patch due to the magnetic vector potential $\boldsymbol{A}$, Φ represents an arbitrary electric scalar potential, and $\boldsymbol{r}$ is a position vector. The first boundary condition on $\boldsymbol{E}$, in terms of $\boldsymbol{A}$ and Φ can easily be found from (13), and it follows that

$$-\hat{\boldsymbol{n}} \text{ x } \boldsymbol{E}^{in}(\boldsymbol{r}) = -\hat{\boldsymbol{n}} \text{ x } \nabla\Phi(\boldsymbol{r}) - i\omega\hat{\boldsymbol{n}} \text{ x } \boldsymbol{A}(\boldsymbol{r}) \tag{14}$$

The magnetic vector potential in (13) is given as

$$\boldsymbol{A}(\boldsymbol{r}) = \int_S \boldsymbol{G}_A(\boldsymbol{r},\boldsymbol{r}') \cdot \boldsymbol{J}_s(\boldsymbol{r}')\, dS \tag{15}$$

where $\boldsymbol{G}_A$ is the dyadic Green's function associated with the magnetic vector potential, $\boldsymbol{J}_s$ is the equivalent current density on the surface of the planar circuit, $\boldsymbol{r}$ is the position vector of the observer and $\boldsymbol{r}'$ is the position vector of the source on the surface S. The electric scalar potential in (13) is given as

$$\Phi(\boldsymbol{r}) = \frac{i}{\omega}\int_S G_p(\boldsymbol{r},\boldsymbol{r}')\,\rho(\boldsymbol{r}')\, dS \tag{16}$$

where G_p is the scalar potential produced by a unit charge associated with horizontal current, and ρ is the charge density is related to the surface divergence of $\boldsymbol{J}_s$, which

given by the continuity equation (7) as

$$\mathbf{V}\cdot\mathbf{J}_s = i\omega\rho \tag{17}$$

Equation (13), with (15) - (17), constitutes the so-called electric field integral equation. One notes that presence of derivatives on the current density in (17) and on the scalar and vector potential in (13) suggests that care should be taken in selecting the basic function and testing procedure.

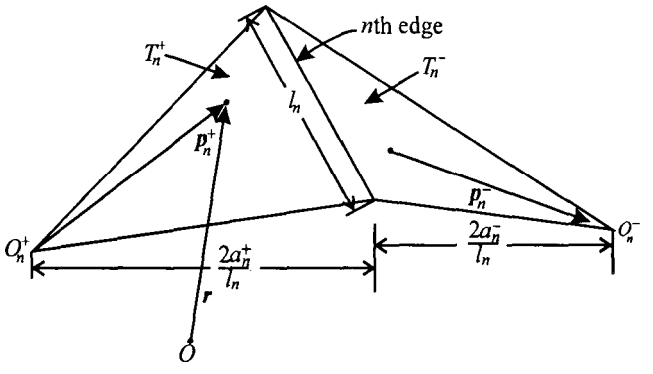

Figure 2. Triangle pair and geometrical parameters associated with the interior edge.

B. Basis Function

An arbitrary closed surface S is given and shown in Figure 1. The surface is first approximated by a number of triangles in Figure 2. Each triangle is defined by an appropriate set of faces, edges and vertices. Figure 2 shows two such triangles, T_n^+ and T_n^- with the nth common edge. The electric and magnetic current flow along radial direction ρ_n^+ in triangle T_n^+ and similarly flow along radial direction ρ_n^+ in triangle T_n^-. Referring to Figure 2, if l_n is the base length of common edge, then height lengths of the two triangles T_n^+ and T_n^- are, respectively, given by $2a_n^+/l_n$ and $2a_n^-/l_n$, where $a_n^\pm$ represents the area of $T_n^\pm$. Any point in triangles $T_n^\pm$ can be defined either with respect to global origin, O, or to the triangle vertices $O_n^\pm$. In Figure 2 the superscripts plus and minus signs designation of the triangles are determined by choice of a positive current reference direction for the nth edge, which is always assumed to be from T_n^+ to T_n^-. Hence, a vector basis function associated with nth edge as

$$f_n(\boldsymbol{r}) = \begin{cases} \frac{l_n}{2a_n^+}\boldsymbol{p}_n^+, \boldsymbol{r} \text{ in } T_n^+ \\ \frac{l_n}{2a_n^-}\boldsymbol{p}_n^-, \boldsymbol{r} \text{ in } T_n^- \\ 0 \quad \text{otherwise.} \end{cases} \tag{18}$$

The unknown current distribution on S is expanded in terms of a set of basis function as

$$\boldsymbol{J}_s(\boldsymbol{r}) = \sum_{n=1}^{N} J_n \boldsymbol{f}_n(\boldsymbol{r}) \tag{19}$$

where N is the number of interior (nonboundary) edges, $\boldsymbol{f}_n(\boldsymbol{r})$ is the vector basis function associated with the nth edge, and the coefficient J_n *can* be interpreted as the current density perpendicular to the edge.

C. Testing Procedure

The **next** step is to test the expansion functions $\boldsymbol{f}_n(\boldsymbol{r})$ developed in [8], which is obtained as follows.

The symmetric product of two vector function f and g is denoted by (f, g), and is defined here to be the surface integral of their scalar product. In other words,

$$\langle \boldsymbol{f}, \boldsymbol{g} \rangle \equiv \int_S \boldsymbol{f} \cdot \boldsymbol{g}\, dS \tag{20}$$

where S denotes the surface where both f and g are non-zero, and (13) is tested with $\boldsymbol{f}_m$, yielding

$$\langle \boldsymbol{E}^{in}, \boldsymbol{f}_m \rangle = i\omega \langle \boldsymbol{A}, \boldsymbol{f}_m \rangle + \langle \nabla\Phi, \boldsymbol{f}_m \rangle \tag{21}$$

Using a surface vector calculus identity and the properties of $\boldsymbol{f}_m$ at the edges of S, the last term in (21) can be written as

$$\langle \nabla\Phi, \boldsymbol{f}_m \rangle = -\int_S \Phi \nabla_S \cdot \boldsymbol{f}_m dS. \tag{22}$$

With the divergence of f,(r) in (1 8), the integral in (22) may now be written and approximated as follows :

$$\int_S \Phi \nabla_S \cdot \boldsymbol{f}_m dS = l_m \left(\frac{1}{a_m^+} \int_{T_m^+} \Phi\, dS - \frac{1}{a_m^-} \int_{T_m^-} \Phi\, dS \right) \cong l_m \left[\Phi(r_m^{C^+}) - \Phi(r_m^{C^-}) \right] \tag{23}$$

In (23) the average of Φ over each triangle is approximated the value at the triangle centroid. With similar approximations, the vector potential and incident field terms in (21) can be written as

$$\left\langle \begin{Bmatrix} \boldsymbol{E}^{in} \\ \boldsymbol{A} \end{Bmatrix}, f_m \right\rangle = \frac{l_m}{2}\left[\frac{1}{a_m^+}\int_{T_m^+} \begin{Bmatrix} \boldsymbol{E}^{in} \\ \boldsymbol{A} \end{Bmatrix} \cdot \boldsymbol{p}_m^+ dS + \frac{1}{a_m^-}\int_{T_m^-} \begin{Bmatrix} \boldsymbol{E}^{in} \\ \boldsymbol{A} \end{Bmatrix} \cdot \boldsymbol{p}_m^- dS \right]$$

$$\cong \frac{l_m}{2}\left[\begin{Bmatrix} \boldsymbol{E}^{in}\left(r_m^{C^+}\right) \\ \boldsymbol{A}\left(r_m^{c^+}\right) \end{Bmatrix} \cdot \boldsymbol{p}_m^{C^+} + \begin{Bmatrix} \boldsymbol{E}^{in}\left(r_m^{C^-}\right) \\ \boldsymbol{A}\left(r_m^{C^-}\right) \end{Bmatrix} \cdot \boldsymbol{p}_m^{C^-} \right] \tag{24}$$

where the integral over each triangle is eliminated by approximating $\boldsymbol{E}^{in}$ (or $\boldsymbol{A}$) by their values at the centroid of each triangle, which is shown in Figure 2. With (22) - (24), (21) now becomes

$$\frac{i\omega l_m}{2}\left[\boldsymbol{A}\left(r_m^{c^+}\right)\cdot \boldsymbol{p}_m^{c^+} + \boldsymbol{A}\left(r_m^{c^-}\right)\cdot \boldsymbol{p}_m^{c^-} \right] + l_m\left[\Phi\left(r_m^{c^-}\right) - \Phi\left(r_m^{c^+}\right) \right]$$

$$= \frac{l_m}{2}\left[\boldsymbol{E}^{in}\left(r_m^{c^+}\right)\cdot \boldsymbol{p}_m^{c^+} + \boldsymbol{E}^{in}\left(r_m^{c^-}\right)\cdot \boldsymbol{p}_m^{c^-} \right] \tag{25}$$

which is the equation enforced at each triangle edge, $m = 1, 2, \ldots, N$

D. Matrix Equation

Substitution of the current expansion in (19) into (25), and the testing is performed, an N x N system of linear equations is obtained and can be written in matrix form as

$$\boldsymbol{ZI} = \mathrm{v} \tag{26}$$

where $\boldsymbol{Z} = [\boldsymbol{Z}_{mn}]$ is a N x N matrix, $Z = [\boldsymbol{I}_n]$ contains the unknown current coefficients J_n which are defined by (19), and $V = [\boldsymbol{V}_m]$ *are* column vectors of length N. The impedance elements $\boldsymbol{Z}_{mn}$ and the voltage elements $\boldsymbol{V}_m$ *are* given by

$$\boldsymbol{Z}_{mn} \approx -\frac{i\omega l_m}{2}\left(\boldsymbol{A}_{mn}^+ \cdot \boldsymbol{p}_m^{c^+} + \boldsymbol{A}_{mn}^- \cdot \boldsymbol{p}_m^{c^-} \right) + \frac{l_m}{i\omega}\left(\Phi_{mn}^- - \Phi_{mn}^+ \right) \tag{27}$$

$$\boldsymbol{V}_m = -\frac{l_m}{2}\left[\boldsymbol{E}^{in}\left(r_m^{c^+}\right)\cdot \boldsymbol{p}_m^{c^+} + \boldsymbol{E}^{in}\left(r_m^{c^-}\right)\cdot \boldsymbol{p}_m^{c^-} \right] \tag{28}$$

where

$$\boldsymbol{A}_{mn}^{\pm} = \int_S G_A\left(r_m^{c^\pm}, r'\right) f_n(r')\, dS' \tag{29}$$

$$\Phi_{mn}^{\pm} = \int_S G_p\left(r_m^{c^\pm}, r'\right) \rho(r')\, dS' \tag{30}$$

where $r_m^{c\pm}$ and $p_m^{c\pm}$ represent the centroid of the triangle $T_m^{\pm}$ associated with the mth edge in the global and local coordinates, respectively.

The Green's functions used in eqns. (29) and (30) have been presented in various method, and should be corrected to get more accurate calculated input impedance. In the present work, the functions given in reference [9] have been adopted

III. NUMERICALRESULTS

In this section, we present some results obtained with present formulation and compare them to measurements and numerical computations that have appeared in the literature [2]-[4],[6], which serve to check the validity of the method, and also to demonstrate its flexibility and efficiency. As an example, the figure 3 shows a Smith chart of impedance loci for a coax-fed square patch. In this example, there are a total of 2 18 triangular faces consisting of 27 1 edges. The unknown normal components of the electric currents are to be solved at the 271 edges. The input impedances that are derived using this method are compared with reference [6]. Very good agreement is achieved by properly locating the position of a coaxial feed probe x_0, as can be seen in Fig. 3. It should be mentioned that the number of triangular elements is determined in such a way that a convergent result can be obtained.

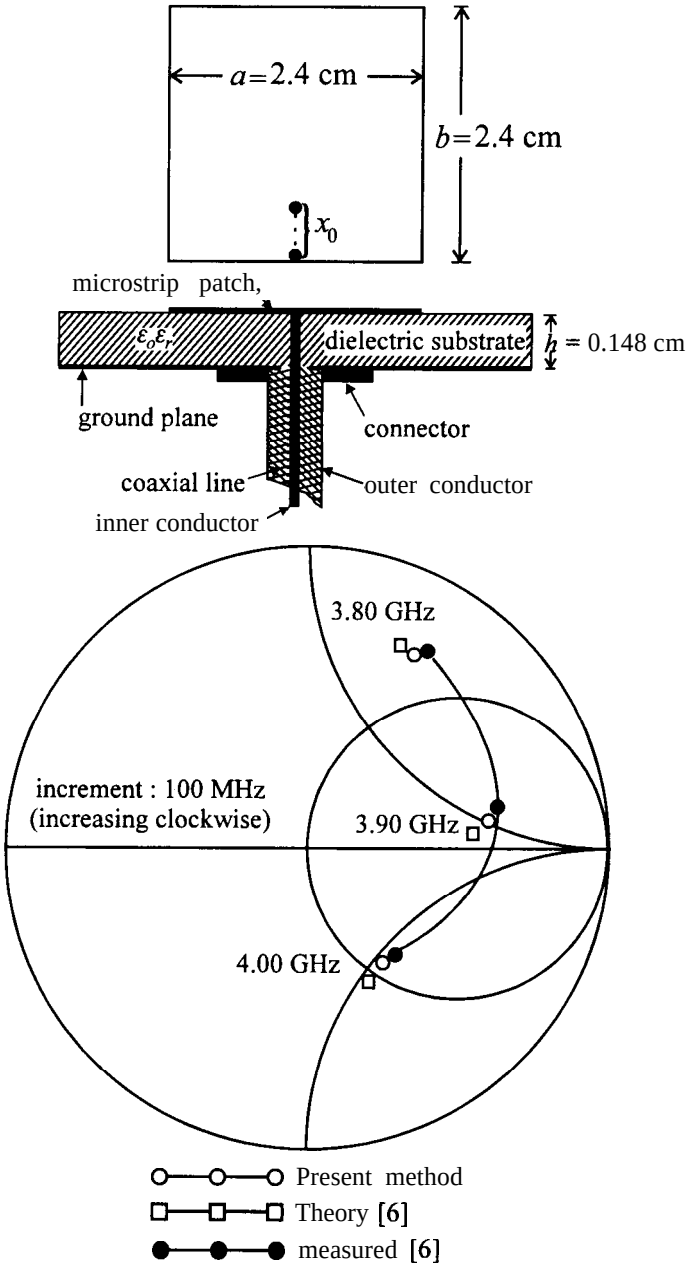

Figure 3. Input impedance of a square patch : a = 2.4 cm, b = 2.4 cm, ε_r = 2.33, tan6 = 0.001, h = 0.148 cm.

The second numerical example, a coax-fed rectangular patch is also analysed. In this example, convergent results are obtained using 258 triangular elements. A comparison of calculated and measured impedance for a coax-fed rectangular patch are shown in Figure 4.

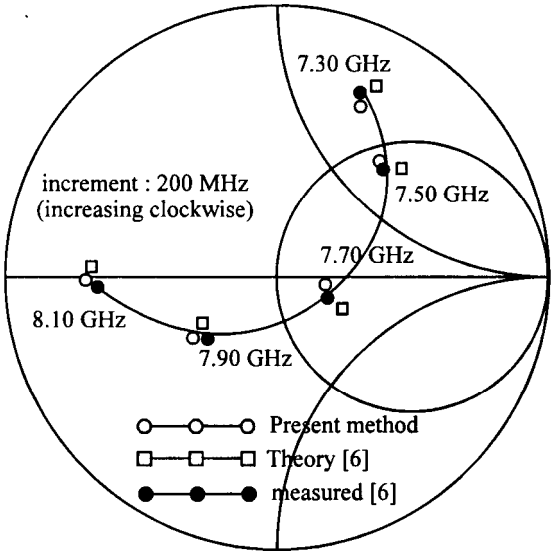

Figure 4. Input impedance of a rectangular patch : a = 2.00 cm, b = 1.25 cm, ε_r = 2.22, $\tan\delta$ = 0.001, h = 0.079 cm.

The third example, the surface of the rectangular patch and its feed-line is modelled in terms of 3 12 triangular elements,which convergent results are obtained. The present method and the calculated results [2],[3] of input impedance for a microstrip line-fed rectangular patch are shown in Figure 5.

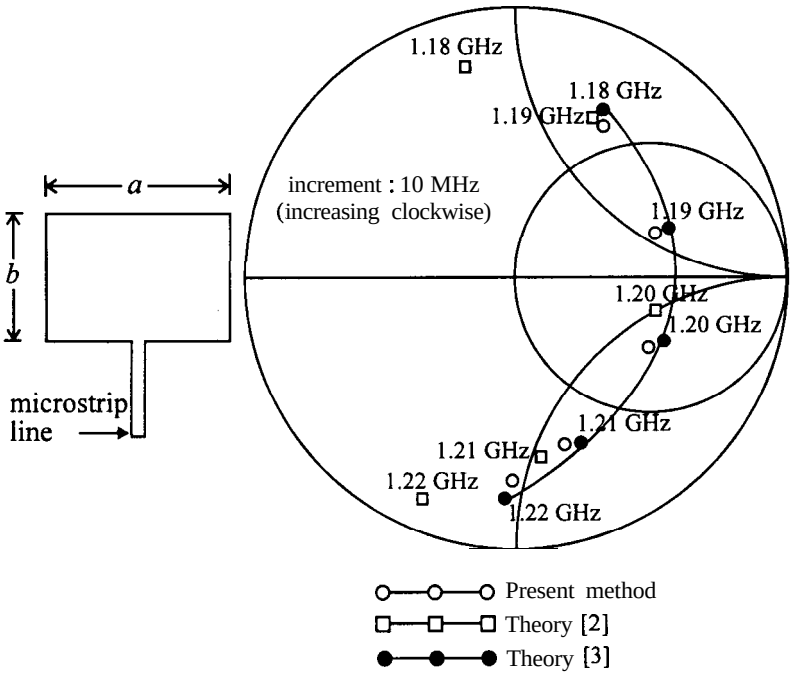

Figure 5. Input impedance of a rectangular patch : a = 11.40, b = 7.6 cm, ε_r = 2.62, tan6 = 0.001, h = 0.159 cm.

In Figure 6, theoretical computations of input impedance are compared in the Smith chart plots with measurements for a coax-fed circular patch. In this example, a total of 345 triangular elements are obtained for convergence.

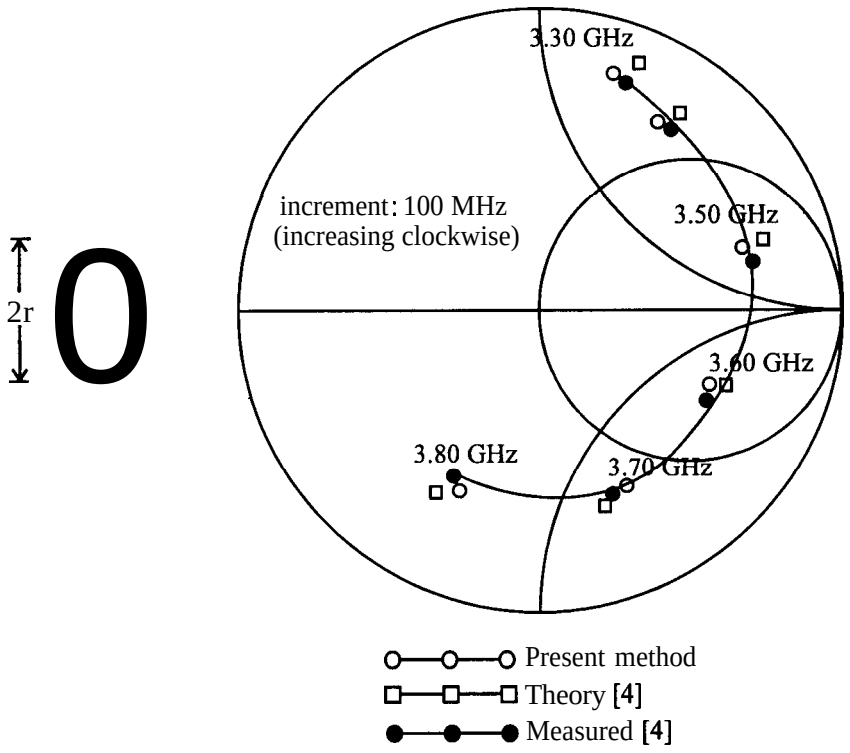

Figure 6. Input impedance of a circular patch : $r =$ 1.41 cm, $\varepsilon_r =$ 2.62, $\tan\delta =$ 0.001, h = 0.16 cm

IV. Conclusion

In this paper a numerical method for the analysis of the input impedance of rectangular, square and circular microstrip antenna, which excited with a coaxial line and a microstrip line, has been presented. It has been shown that the FEM is a very powerful tool for analyzing the planar microstrip patch modeled with triangular patches. The method can be used to accurately predict the input impedance of all antenna shapes. The validity of the model is demonstrated by comparing the numerical and experimental results for four representative antenna structures.

ACKNOWLEDGMENT

The author would like to thank with Mr. Nimit Tummaprasert who made many helpful calculations, editions, comments and suggested the example of a convergence. The author also would like to thank reviewers for their valuable advice and helpful corrections to the grammer.

REFERENCES

[1] K.R. Carver and J.W. Ming, "Microstrip antenna technology," *IEEE Trans. Antennas Propagat.*, vol. AP-29, no. 1, pp. 2-23, Jan. 1981.

[2] E.H. Newman and P. Tulyathan, "Analysis of microstrip antennas using moment methods," *IEEE Trans. Antennas Propagat.*, vol. AP-29, no. 1, pp. 47-53, Jan. 1981.

[3] M.D. Deshpande and M.C. Bailey, "Input impedance of microstrip antennas," *IEEE Trans. Antennas Propagat.*, vol. AP-30, no. 4, pp. 645-650, July 1982.

[4] M Davidovitz and Y.T. Lo, "Input impedance of a probe-fed circular microstrip antenna with thick substrate," *IEEE Trans. Antennas Propugat*, vol. AP-34, no. 7, pp. 905-911, July 1986.

[5] D.M. Pozar and S.M. Voda, "A rigorous analysis of a microstripline fed patch antenna," *IEEE Trans. Antennas Propagat.*, vol. AP-35, no. 12, pp. 2343 - 1350, Dec. 1987.

[6] J.P. Damino and A. Papiernik, "Survey of analytical and numerical models for probe-fed microstrip antennas," *IEE Proc. Microwave Antennas Propa.*, vol. 141, no. 1, pp. 15-22, Feb. 1994.

[7] C.A. Balanis, *Antenna Theory* : Analysis and Design, Harper & Row, Publishers, Inc. 1982.

[8] K. Umashankar, A Taflove and S.M. Rao, "Electromagnetic scatting by arbitrary shaped three-dimensional homogeneous lossy dielectric objects," *IEEE Trans. Antennas Propagat.*, vol. AP-34, no. 4, pp. 758-766, June 1986.

[9] D.G. Fang, J.J. Yang, and G.Y. Delisle, "Discrete image theory for horizontal electric dipoles in a multilayered medium," *IEE Proc. Microw. Antennas Propag.* vol. 135, no. 5, pp. 297-303, Oct. 1988.